

1 **REVISION 1**

2
3 **The Incompressibility of Atoms at High Pressures**

4
5
6 Gerald V. Gibbs¹, David F. Cox², Nancy L. Ross^{1*}

7
8 ¹ Department of Geosciences, Virginia Tech, Blacksburg, VA 24061, USA

9 ² Department of Chemical Engineering, Virginia Tech, Blacksburg, VA 24061,

10
11
12 **Abstract**

13
14
15 The structures of the silica polymorphs α -quartz and stishovite have been geometry optimized at
16 high simulated, isotropic pressure within the framework of Density Functional Theory. The
17 atoms of the high pressure polymorph stishovite are virtually incompressible with the bonded
18 radii for Si and O atoms decreasing by only 0.04 Å and 0.08 Å, respectively, at 100 GPa. In
19 compensating for the increase in the effective interatomic potential associated with the
20 compression of the Si-O bonded interactions, the electron density at the bond critical point
21 between the bonded pair increases from 0.69 e/Å³ to 0.89 e/Å³. The bonded radii of the Si and O
22 atoms for α -quartz decrease by 0.006 Å and 0.008 Å, respectively, between 1 bar and 26.4 GPa.
23 The impact of simulated, isotropic pressure on the bonded radii of the atoms for three perovskites
24 YAIO₃, LaAlO₃ and CaSnO₃ was also examined at high pressure. For the YAIO₃ perovskite, the
25 bonded radii for Y and Al decrease by 0.06 Å and 0.05 Å, respectively, at 80 GPa while the
26 electron density between the bonded atoms increases by 0.12 e/Å³ and 0.15 e/Å³, on average.
27 The calculations also show that the coordination number of the Y atom increases from 9 to 10
28 while the coordination number of the O1 atom increases concomitantly in the structure from 5 to
29 6 at 20 GPa. Hence pressure not only promotes an increase in the coordination number of the
30 metal atoms but also a necessary concomitant increase in the coordination number of the O

31 atoms. The bonded radii, determined at a lower pressure between 0.0 and 15 GPa for LaAlO₃ and
32 CaSnO₃, decrease a smaller amount with the radii for the La and Ca atoms decreasing by 0.03 Å
33 and 0.04 Å, respectively, while the radii for the smaller Al and Sn atoms decrease by 0.01 Å and
34 0.02 Å, respectively. In general, O atoms are more compressible than the metal atoms but
35 overall, the calculations demonstrate that the bonded radii for the atoms in crystals are virtually
36 incompressible when subjected to high pressure. The reason that the bonded radii change little
37 when subjected to high pressure is ascribed to the changes in the effective interatomic potentials
38 that result in increased repulsion when the atoms are squeezed together.

39

40

41

42

43

44

45

46

47

48

49

50

51

52

53

54

55

56

57

58

59

60

61

62

63

64

65

Keywords: High pressure, bonded radii, silica polymorphs, perovskites

66
67
68
69
70
71
72
73
74
75
76
77
78
79
80
81
82
83
84
85
86
87
88
89
90

Introduction

To appreciate the impact of pressure on the structure and crystal chemistry of an oxide crystal, it is important, as argued by Prewitt and Downs (1998), that we understand the impact of pressure on the oxide anions, the bonded cations and the cation containing coordination polyhedra. They also argued that coordinated polyhedra, containing large cations with small valences can be expected to be more compressible than those containing smaller cations with larger valences. Based on an examination of several experimental electron density maps determined by Sasaki et al. (1980), they also suggested that the atomic nuclei of the individual ions of an oxide crystal are shrouded by incompressible spherical cores of electron density that in turn are enclosed by more compressible, low lying shells. On the basis of this suggestion, they argued that the outer shells of the ions are ideal regions where the compressibility of a crystal may be accommodated. These arguments, combined with results of density functional theory (DFT) calculations for the silica polymorphs (Nicoll et al., 1994) and force constants estimated for the bonded interactions for a number of oxide molecules (Hill et al., 1994), Prewitt and Downs (1998) developed guidelines as to how the sizes of the ions, the bond lengths and the coordination numbers of the atoms of a material may be expected to respond to pressure. These guidelines include: (1) Longer bonded interactions are more likely to decrease than shorter stronger ones; (2) The shared character of a bonded interaction increases with decreasing bond length, (3) The coordination number of a cation increases upon compression and (4) Oxygen anions are more compressible than metal cations. Grochala et al. (2007) have since examined the rules for a variety of materials, ranging from molecules to metals, with atoms that they considered to be in ‘very tight places’, that is, at pressures ranging up to that at the center of the Earth, 380 GPa. Despite the relative simplicity of

91 the rules, they observed that the Prewitt and Downs (1998) rules are quite correct and serve as
92 useful constructs for understanding how the structures and bonded interactions for a variety of
93 materials respond to high pressure.

94
95 In this study, we have determined the impact of pressure on the sizes of the bonded radii of the
96 atoms and the polarization of the electron density distributions for two polymorphs of SiO₂ with
97 different structures and coordination numbers and three metal-oxide perovskites with similar
98 structures but different compositions. We used the approach of Bader and his colleagues (Bader,
99 1985; Runtz et al., 1977) who examined the electron density distribution for a number of
100 molecules in a search for a feature that may serve and qualify as a bonded interaction. In the
101 search, they discovered that adjacent atoms that were possibly bonded were connected by well-
102 defined continuous pathways of maximum electron density. Furthermore, the value of the
103 electron density along the paths was found to decrease systematically from the nucleus of each
104 pair to a local minimum in the electron density along the path where the gradient of the electron
105 density is zero. The pathway of maximum electron density that connects the nuclei of the pair
106 was denoted the bond path of the interaction and the point along the path where the electron
107 density adopts a minimum value was denoted the bond critical point, r_c . Later, based on the
108 topological properties of the electron density, Bader (2009) concluded that two atoms, M and O,
109 are necessarily bonded only if the pair is connected by a bond path. In addition, he asserted that
110 ‘One may define the bond path operator as a Dirac observable, making the bond path a
111 measurable expectation value of a quantum mechanical operator.’ The distances between the
112 nuclei of the pair and the point along the path where the electron density adopts a minimum
113 value, define the bonded radii for the pair of bonded atoms, M and O, denoted $r_b(M)$ and $r_b(O)$. It

114 was also observed that when the bonded radius sum of the bonded pair, $r_b(M) + r_b(O)$, matches
115 the length of the bonded interaction, denoted, $R(M-O)$, then the M-O bonded interaction is
116 assumed to be a stable and strain free interaction (Bader, 1990; Bader and Matta, 2004).

117
118 In a recent study of electron density distributions, Gibbs et al. (2013) calculated the bonded radii
119 for first, second and third row atoms at ambient conditions, for a relatively large number of
120 crystals. At odds with the assumption that the Shannon and Prewitt (1969) crystal radius of the
121 oxide anion shows little or no change when bonded, it was found that the bonded radii for the O
122 atom decrease systematically from 1.40 Å when bonded to an electropositive atom like
123 potassium to 0.60 Å when bonded to a more electronegative atom like nitrogen. Further, the
124 bonded radii for the more electropositive metal atoms agree with the crystal radii where the
125 electron density distribution of the O atom is largely unpolarized. But the bonded radii for the
126 more electronegative metal atoms are progressively larger than the crystal radii as the electron
127 density is progressively contracted along bond paths of the bonded interactions. This study
128 prompted further scrutiny of the effect of pressure on the oxide anion, the bonded cations and the
129 cation containing coordination polyhedra for different structures.

130
131 With this approach, the impact of simulated isotropic pressures as high as 100 GPa and its effect
132 on the electron density distributions of the silica polymorphs α -quartz (Gibbs et al., 1999) and
133 stishovite and three perovskites of $LaAlO_3$, $CaSnO_3$ and $YAlO_3$ composition (Gibbs et al., 2012;
134 Wang, 2012) were examined. The calculations were completed within the framework of density
135 functional theory, followed by a determination of the electron density distributions, the bond
136 paths and the bond critical points properties for the bonded interactions (Bader, 2009). In short,

137 rather than examining how the crystal radii of the atoms are impacted for a range of pressures,
138 we describe how the bonded radii are impacted by pressure as it would be very time consuming
139 task to determine how the crystal radii for a variety of crystal structures respond to high pressure.
140 We also examined the extent to which the Prewitt-Downs rules hold in terms of how the bond
141 lengths, and the compressibilities, χ , of the bonded atoms respond to pressure.

142

143 **The impact of isotropic pressure on the bonded radii of the atoms of α -quartz and** 144 **stishovite**

145
146 The structure of the silica polymorph α -quartz consists of a 3D array of corner sharing SiO_4
147 silicate tetrahedral oxyanions such that each O atom is bonded to two Si atoms and each Si atom
148 is bonded to four O atoms. The number of bond paths and resulting coordination number of the
149 O atoms is 6 thus the complete structural formula is ${}^{\text{iv}}\text{Si}^{\text{ii}}\text{O}_2$ and Hosler's Rule holds as $4*1 =$
150 $2*2$. On the other hand, the structure of the high pressure polymorph, stishovite, consists of a 3D
151 array of corner- and edge-sharing SiO_6 octahedral oxyanions such that each O atom is bonded to
152 three Si atoms and each Si atom is bonded to six O atoms. Thus the complete structural formula
153 for stishovite is ${}^{\text{vi}}\text{Si}^{\text{iii}}\text{O}_2$ and Hosler's Rule holds as $6*1 = 2*3$. As the ${}^{\text{vi}}\text{Si}$ and ${}^{\text{iii}}\text{O}$ atoms for
154 stishovite are six and three coordinated, respectively, and the ${}^{\text{iv}}\text{Si}$ and ${}^{\text{ii}}\text{O}$ in quartz are four and
155 two coordinated, respectively, the ${}^{\text{vi}}\text{Si} - {}^{\text{iii}}\text{O}$ bond length in stishovite is necessarily longer, 1.75 Å,
156 than the ${}^{\text{iv}}\text{Si} - {}^{\text{ii}}\text{O}$ bond length, 1.61 Å, recorded at ambient conditions. The bonded radii for the Si
157 and O atoms, $r_b(\text{Si})$ and $r_b(\text{O})$, respectively, for both α -quartz and stishovite are displayed in
158 Figure 1, as determined within the framework of DFT as a function of isotropic pressure (Gibbs
159 et al., 1999). The observation that the sum of the bonded radii, $r_b(\text{Si}) + r_b(\text{O})$, for both silica
160 polymorphs, equals the corresponding Si-O bond lengths at pressure, satisfies the constraint that
161 the Si-O bonded interactions are stable and strain free.

162
163 The compression mechanism in α -quartz differs substantially from that of stishovite. In α -quartz,
164 the volume reduction at high pressure is achieved by the bending of the compliant Si-O-Si angles
165 that connect the rigid SiO₄ tetrahedra (Hazen et al., 1989). In stishovite, the major compression
166 mechanism involves reduction of the relatively stiff Si-O bonded interactions, especially the
167 longer Si-O apical bonds in the structure (Ross et al., 1990). The difference in compression
168 mechanisms is reflected in the differing in their bulk modulus. Quartz has a relatively small bulk
169 modulus of 37 GPa (Angel et al., 1997) while stishovite has a substantially greater bulk modulus
170 of 306 GPa (Ross et al., 1990).

171
172 As evinced by Figure 1, the O atoms are more compressible, χ , than the Si atoms, in agreement
173 the Prewitt-Downs (1998) rule that O atoms are more compressible than metal atoms. In the case
174 of α -quartz, the value of $r_b(\text{Si})$ decreasing $\chi \approx -1.95 \times 10^{-4} \text{ \AA/GPa}$ with increasing pressure with
175 $r_b(\text{O})$ decreasing, $\chi \approx -3.40 \times 10^{-4} \text{ \AA/GPa}$, whereas in the case of stishovite, $r_b(\text{Si})$ decreases more,
176 $\chi \approx -3.9 \times 10^{-4} \text{ \AA/GPa}$, while $r_b(\text{O})$ decreases even more, $\chi \approx -8.4 \times 10^{-4} \text{ \AA/GPa}$, assuming that the
177 radii for both silica polymorphs decreasing roughly linearly with increasing pressure. As such,
178 the bonded radius for the larger O atom in stishovite decreasing ~ 2.5 times more than the smaller
179 O atom in α -quartz, upon being compressed, whereas the larger Si atom in stishovite decreases
180 twice as much as the smaller Si atom in α -quartz. As expected, the Si-O bonded interaction,
181 $\sim 1.60 \text{ \AA}$, for α -quartz decreases less than the longer and weaker Si-O bond length optimized for
182 stishovite, $\sim 1.75 \text{ \AA}$. Overall, the relatively small decrease in the bonded radii for the Si and O
183 atoms, particularly encountered in the case of stishovite at 100 GPa, is ascribed to a change in
184 the effective interatomic potential between the Si and O atoms upon compression. As discussed

185 in detail by Prencipe and Nestola (2006), the effective interatomic potential is the sum of the
186 Coulomb potential and the kinetic energy of the electrons. The latter increases strongly when the
187 electrons are confined in increasingly smaller volumes with the result that there is an increase of
188 the effective potential as the atoms are squeezed together that increases, in turn, the repulsions
189 between them. In addition, Grochala et al. (2007) asserted that the electron density between a
190 pair of bonded atoms when subjected to pressure, must necessarily be modified upon being
191 compressed. It does so for the silica polymorphs with a migration of electron density into the
192 internuclear region between the compressed bonded atoms, shielding the nuclei of the atoms. In
193 the case of stishovite, this is borne out with a concomitant and progressive increase in the
194 accumulation of the electron density, $\rho(\mathbf{r}_c)$, at the bond critical point, \mathbf{r}_c , between the bonded Si
195 and O atoms. The $\rho(\mathbf{r}_c)$ -values for the Si-O bonded interactions for α -quartz likewise increase
196 with increasing pressure with the Si-O bonds for both α -quartz and stishovite becoming more
197 shared in character with increasing pressure, in agreement with Prewitt and Downs (1998) rule
198 that the shared character of a bonded interaction increases when a bonded interaction is
199 compressed. These results suggest that a metal atom coordinated by a larger number of O atoms
200 is more compressible than an atom coordinated by a smaller number of O atoms. It also suggests
201 the coordinating O atoms are likewise more compressible than the smaller Si atoms

202

203 **The impact of pressure on the bonded radii of the atoms for the perovskites**

204 The ideal perovskite structure with ABO_3 stoichiometry has cubic symmetry ($Pm\bar{3}m$) and
205 consists of corner-sharing BO_6 octahedra with larger A cations filling the cavities within the
206 octahedral framework. Perovskites can attain a variety of symmetries due to tilting of the
207 octahedra that can result in a change of the coordination of the A cation from the ideal 12-fold

208 coordination with oxygen of the cubic prototype structure (Glazer, 1972; Woodward, 1997). For
209 example, LaAlO₃ is rhombohedral (R-3c) and bond paths connect each of the La and Al atoms
210 with O atoms. Six bond paths are found to extend between the Al atoms to nearest-neighbor O
211 atoms at 0 GPa verifying its coordination number is six. Twelve bond paths are found to extend
212 between the La atoms and nearest-neighbor oxygen atoms so the coordination of La is
213 determined to be twelve at 0 GPa. The number of bond paths and resulting coordination number
214 of the O atoms is 6 thus the complete structural formula is ^{xii}La^{vi}Al^{vi}O₃ and Hosler's Rule holds
215 as $12*1 + 6*1 = 6*3$. At high pressure, the rotation angle around the threefold axis of the AlO₆
216 octahedra is determined by the relative compressibilities of the LaO₁₂ and AlO₆ sites. Zhao et al.
217 (Zhao et al., 2004) observed that the rotation angle decreases significantly with pressure,
218 ultimately leading to a phase transition from rhombohedral symmetry to cubic symmetry at high
219 pressure.

220 In contrast to LaAlO₃ perovskite, CaSnO₃ and YAlO₃ are orthorhombic (*Pbnm*). Bond paths
221 connect each of the Ca, Sn, Y and Al atoms with O atoms. The Ca-O, Sn-O, Y-O and Al-O
222 linkages for the three perovskites are therefore considered to be necessarily bonded interactions
223 (Bader, 2009). In this study, six bond paths are found to extend between the Sn atoms to nearest-
224 neighbor oxygen atoms in CaSnO₃ at 0 GPa verifying its coordination number of 6. Eight bond
225 paths are found to extend between the Ca atoms to nearest-neighbor oxygen atoms so the
226 coordination of Ca is determined to be eight. The bond paths and coordination numbers of the O₁
227 and O₂ atoms are 4 and 5, respectively, thus the complete structural formula is ^{xiii}Ca^{vi}Sn^{iv}O₁^vO₂
228 and Hosler's Rule holds as $8*1 + 6*1 = 4*1 + 5*2$. In YAlO₃, six bond paths are found to extend
229 between the Al atoms to nearest-neighbor oxygen atoms at 0 GPa verifying its coordination
230 number is 6. In contrast to CaSnO₃, nine bond paths are found to extend between the Y atoms

231 and nearest-neighbor oxygen atoms so the coordination of Y is determined to be nine at 0 GPa.
232 The number of bond paths and coordination numbers of the O1 and O2 atoms in $YAlO_3$ are both
233 5, thus the complete structural formula is ${}^{ix}Y^{vi}Al^vO_1^vO_2$ and Hosler's Rule holds as $9*1 + 6*1 =$
234 $5*1 + 5*2$. High-pressure single-crystal X-ray experiments show that the structures of $CaSnO_3$
235 and $YAlO_3$ undergo a different structural response to pressure. In the II-IV perovskite, $CaSnO_3$,
236 the SnO_6 octahedra are less compressible than the CaO_8 sites with the result that the structure
237 becomes more distorted with pressure (Zhao et al., 2004). In the III-III perovskite, $YAlO_3$, the
238 AlO_6 site is more compressible than the YO_9 site so the structure becomes less distorted with
239 pressure (Ross et al., 2004).

240 To understand how the bonded radii of the atoms for the three perovskites respond to pressure,
241 we examined the results of high-pressure DFT simulations (Gibbs et al., 2012; Wang, 2012). The
242 structures of $LaAlO_3$ and $CaSnO_3$ were determined at a continuum of simulated isotropic
243 pressures, ranging between 0.0 GPa and 15.0 GPa. On the other hand, the structure of the $YAlO_3$
244 perovskite was geometry optimized for a wider range of pressures, between 0 GPa and 80 GPa.
245 Below we describe the impact of pressure on the bonded radii for each of the La, Y, Ca, Sn, Al
246 and O atoms in these three perovskites.

247 **Impact of simulated pressure on radii of the atoms in $LaAlO_3$ perovskite**

248 Details of the bonded radii, $r_b(La)$, $r_b(Al)$, and $r_b(O)$, and the electron density at the bond critical
249 point ($\rho(r_c)$) generated for the nonequivalent atoms for the $LaAlO_3$ perovskite for pressures
250 between 0.0 and 15 GPa are given in Table 1 (see (Gibbs et al., 2012) for the nomenclature of the
251 atoms for the perovskites). In the case of the La–O_i bonded interactions, the bonded radii for
252 both $r_b(La)$ and $r_b(O_i)$ display anomalies: both unexpectedly increasing slightly, 0.003 Å, rather
253 than decreasing with increasing pressure (Fig. 2). The value of $\rho(r_c)$ of R(La–O_i) shows no

254 change between 0.0 and 15 GPa (Table1). As $R(\text{La} - \text{O}_i) = r_b(\text{La}) + r_b(\text{O}_i)$, the La - O_i bonded
255 interaction is indicated to be stable and free of strain despite the increase in bond length. As
256 such, they are stable bond lengths and bonded radii as they both show a slight increase with
257 increasing pressure. However, as described below, the remaining La-O bonded interactions, La –
258 O_{ii} and La –O_{iii}, both decrease with increasing pressure (Fig. 2). The Al-O bond lengths in
259 LaAlO₃ also decrease with increasing pressure (Table 1).

260 For the La – O_{ii} bonded interaction, $R(\text{La} - \text{O}_{ii}) = 2.656 \text{ \AA}$ with $r_b(\text{La}) = 1.431 \text{ \AA}$ and $r_b(\text{O}_{ii}) =$
261 1.225 \AA at 0.0 GPa. At 15 GPa, the bonded interaction decreases to 2.600 \AA with $r_b(\text{La}) = 1.407$
262 \AA and $r_b(\text{O}_{ii}) = 1.193 \text{ \AA}$ and $\rho(r_c)$ increases slightly (Table 1). Similar results are seen for the La
263 – O_{iii} bonded interaction (Table 1). The compressibilities of the bonded radii are $\chi \approx r_b(\text{La}) = -$
264 $1.6 \times 10^{-3} \text{ \AA / GPa}$, $\chi(r_b(\text{O}_{ii})) = -2.13 \times 10^{-3} \text{ \AA / GPa}$ for $R(\text{La}-\text{O}_{ii})$, and $\chi(r_b(\text{La})) = -3.3 \times 10^{-3} \text{ \AA}$
265 $/\text{GPa}$ and $\chi(r_b(\text{O}_{ii})) \approx -4.7 \times 10^{-3} \text{ \AA / GPa}$ for $R(\text{La}-\text{O}_{iii})$. On the basis of the bonded radii for the
266 La atom, the bonded radius of the atom is 1.42 \AA and that of the O atom bonded to the La atom is
267 1.21 \AA .

268 In the case of the Al atom, $R(\text{Al}-\text{O})$ decreases from 1.886 \AA to 1.842 \AA , $r_b(\text{Al})$ decreases by
269 0.014 \AA between 0.0 and 15 GPa resulting in a smaller compressibility, $\chi(r_b(\text{Al})) \approx -9.3 \times 10^{-4} \text{ \AA}$
270 $/\text{GPa}$. The bonded radius of the O bonded to the Al atom, $r_b(\text{O})$ decreases 0.029 \AA with $\chi(r_b(\text{O})) \approx$
271 $-1.9 \times 10^{-3} \text{ \AA / GPa}$. Thus the compressibility of the Al atom is substantially less than the O atom
272 bonded to the Al.

273 The values of $r_b(\text{Al})$ and $r_b(\text{O})$ determined at $P = 0.0$, 0.791 \AA and 1.095 \AA , respectively, match
274 those determined earlier (0.80 \AA and 1.12 \AA , respectively by (Gibbs et al., 2012). At $P = 0.0$
275 GPa, the value of $r_b(\text{O})$ ranges between 1.13 \AA and 1.33 \AA with an average value of 1.23 \AA
276 whereas the value of $r_b(\text{La})$ ranges between 1.35 \AA and 1.51 \AA with an average value of 1.43 \AA .

277 As $r_b(\text{Al}) + r_b(\text{O}) = 1.886 \text{ \AA}$, the (Al-O) bonded interactions is considered to be stable. The
278 geometry optimized bond lengths, $R(\text{M-O})$, determined for the geometry optimized structures,
279 plotted in Figure 3 in terms of $r_b(\text{M}) + r_b(\text{O})$ for the La and Al atoms, scatter along a line, as
280 anticipated for stable bonded interactions (Fig. 3). The average compressibilities for the larger La
281 atoms is less than that for the O atoms but substantially greater than that for the smaller Al atom,
282 demonstrating that larger metals atom are more compressible than smaller ones.

283

284 **Impact of isotropic pressure on the bonded radii of the atoms for CaSnO_3 perovskite**

285 Details of the nonequivalent bonded radii for the Ca, Sn, O_1 and O_2 atoms for CaSnO_3
286 perovskite and the values of $\rho(\mathbf{r}_c)$ for pressures that range between 0.0 GPa and 15.0 GPa are
287 given in Table 2. As shown in Figure 4, the Ca - O_1 and Ca- O_2 bond lengths and the bonded
288 radii decrease with increasing pressure. The bonded radii of the Ca atom, $r_b(\text{Ca})$, at $P = 0.0$,
289 range between 1.147 and 1.360 \AA with an average value of 1.22 \AA , taken as an estimate of the
290 bonded radius of the Ca atom, compared with 1.25 \AA determined by Gibbs et al. (2013). The
291 bonded radii of the O_1 and O_2 atoms at 0.0 GPa range between 1.13 \AA and 1.44 \AA , with an
292 averaged value of 1.24 \AA , compared with 1.26 \AA , the value determined for the O atom bonded to
293 Ca (Gibbs et al., 2013). For all of the Ca-O bonded interactions, $\rho(\mathbf{r}_c)$ increase with pressure. The
294 compressibilities of the Ca atom, range roughly between $\chi \approx -1.73 \times 10^{-3} \text{ \AA} / \text{GPa}$ and $-2.27 \times 10^{-3} \text{ \AA}$
295 $/\text{GPa}$ with an average value of $-1.99 \times 10^{-3} \text{ \AA} / \text{GPa}$, smaller than that determined for the O atoms
296 bonded to the Ca atom that range between $\chi \approx -2.7 \times 10^{-3} \text{ \AA} / \text{GPa}$ and $\chi \approx -3.8 \times 10^{-3} \text{ \AA} / \text{GPa}$ with an
297 average compressibility value of $\chi \approx -2.94 \times 10^{-3} \text{ \AA} / \text{GPa}$ (Table 2).

298 The two nonequivalent Sn-O bond lengths and the bonded radii for the Sn and O_1 and O_2 atoms
299 likewise decrease with the increasing pressure (Table 2). The three nonequivalent Sn-O bond

300 lengths, $R(\text{Sn}-\text{O1}) = 2.068 \text{ \AA}$, $R(\text{Sn}-\text{O2i}) = 2.068 \text{ \AA}$, $R(\text{Sn}-\text{O2ii}) = 2.064 \text{ \AA}$ are virtually
301 identical at $P = 0 \text{ GPa}$, with an average bonded radii of $r_b(\text{Sn}) = 1.07 \text{ \AA}$ and $r_b(\text{O}) = 1.01 \text{ \AA}$. The
302 values of $\rho(r_c)$ for all of the Sn-O bonded interactions increase slightly with pressure. The
303 compressibilities of the Sn atoms range between $-1.20 \times 10^{-3} \text{ \AA/GPa}$ and $-1.4 \times 10^{-3} \text{ \AA/GPa}$ while
304 those of the O atoms bonded to the Sn atoms are larger and range between $-1.4 \times 10^{-3} \text{ \AA/GPa}$ and
305 $-1.67 \times 10^{-3} \text{ \AA/GPa}$. The bonded interactions for CaSnO_3 are considered to be stable, as evinced by
306 Figure 5 which shows that the sum of the bonded radii matches the bond length for the bonded
307 pair.

308 **Impact of simulated isotropic pressure on the radii of the atoms for the YAlO_3 perovskite**

309 The bonded radii for the Y, Al, O₁ and O₂ atoms for YAlO_3 perovskite and the values of $\rho(r_c)$
310 bonded radii for the atoms of the YAlO_3 perovskite, calculated for a larger continuum of
311 pressures between $P = 0.0 \text{ GPa}$ and 80 GPa are given in Table 3. As described below, the
312 coordination number of the Y atom in the YAlO_3 perovskite increases at 20 GPa from 9 to 10 in
313 agreement with the Prewitt and Down's (1998) observation that high pressure favors structures
314 with larger metal coordination numbers. It also suggests, however, that the coordination number
315 of the larger cations in a structure are more susceptible to increase than the smaller ones. In
316 addition, the coordination number of the O₁ oxygen atom increases concomitantly from five to
317 six.

318 As shown in in Figure 6, six of the seven nonequivalent Y-O bond lengths and associated bonded
319 radii for the of Y and O atoms decrease as the pressure is increases from 0.0 GPa to 80 GPa .
320 $R(\text{Y}-\text{O1i})$, for example, decreases from 2.2213 \AA to 2.0975 \AA , with $r_b(\text{Y})$ decreasing from 1.165
321 \AA to 1.107 \AA . $\chi \approx -7.3 \times 10^{-4} \text{ \AA/GPa}$; $r_b(\text{O1i})$ decreases from 1.056 \AA to 0.991 \AA , $\chi \approx -8.1 \times 10^{-}$
322 4 \AA/GPa . Similar results are observed for $R(\text{Y}-\text{O1ii})$ with $\chi \approx -1.9 \times 10^{-4} \text{ \AA/GPa}$ and $\chi \approx -2.4 \times 10^{-}$

323 $\text{\AA}/\text{GPa}$ for $r_b(\text{Y})$ and $r_b(\text{O1ii})$, respectively. For $R(\text{Y-O1iii})$, $\chi \approx -1.11 \times 10^{-3} \text{\AA}/\text{GPa}$ and $\chi \approx -1.21$
324 $\times 10^{-3} \text{\AA}/\text{GPa}$ for $r_b(\text{Y})$ and $r_b(\text{O1iii})$ (Table 3). For $R(\text{Y-O2i})$, $\chi \approx -7.5 \times 10^{-4} \text{\AA}/\text{GPa}$ for $r_b(\text{Y})$
325 and $\chi \approx -8.8 \times 10^{-4} \text{\AA}/\text{GPa}$ for $r_b(\text{O2i})$. For $R(\text{Y-O2ii})$ $\chi \approx -6.8 \times 10^{-4} \text{\AA}/\text{GPa}$ for $r_b(\text{Y})$ and $\chi = -$
326 $8.8 \times 10^{-4} \text{\AA}/\text{GPa}$ for $r_b(\text{O2ii})$. For $R(\text{Y-O2iii})$, $\chi \approx -8.1 \times 10^{-4} \text{\AA}/\text{GPa}$ for $r_b(\text{Y})$ and $\chi \approx -1.12 \times 10^{-}$
327 $3 \text{\AA}/\text{GPa}$ for $r_b(\text{O2iii})$. At 20 GPa, the number of bonded interactions from Y to O changes from 6
328 to 7 (Fig. 6). The seventh nonequivalent Y-O bond length, $R(\text{Y-O1iv})$, that forms at 20 GPa, is
329 substantially longer than the others and exists up to 80 GPa. From $P = 20.0$ to 80.0 GPa, $R(\text{Y-}$
330 $\text{O1iv})$ decreases from 2.947 \AA to 2.604 \AA ; $r_b(\text{Y})$, 1.485 to 1.334 \AA , $\chi \approx -2.5 \times 10^{-4} \text{\AA}/\text{GPa}$; $r_b(\text{O2iv})$
331 , 1.478 \AA to 1.334 \AA with $\chi \approx -2.4 \times 10^{-3} \text{\AA}/\text{GPa}$.

332 The three nonequivalent Al-O bond lengths are substantially shorter than the Y-O bond lengths
333 and decrease substantially less with increasing pressure from 0.0 to 80 GPa (Table 3). $R(\text{Al -}$
334 $\text{O1})$, for example, decreases from 1.886 \AA to 1.736 \AA with $r_b(\text{viAl})$ decreasing from 0.790 to
335 0.742 \AA , ($\chi = -6.0 \times 10^{-4} \text{\AA}/\text{GPa}$) and $r_b(\text{O1})$ decreasing from 1.096 \AA to 0.994 \AA ($\chi \approx -1.3 \times 10^{-3}$
336 $\text{\AA}/\text{GPa}$). For $R(\text{Al-O2i})$ $\chi \approx -6.2 \times 10^{-4} \text{\AA}/\text{GPa}$ for $r_b(\text{viAl})$ and $\chi \approx -1.3 \times 10^{-3} \text{\AA}/\text{GPa}$ for $r_b(\text{O2i})$.
337 Lastly, for $R(\text{Al-O2ii})$ $r_b(\text{Al})$ $\chi \approx -6.9 \times 10^{-4} \text{\AA}/\text{GPa}$ for $r_b(\text{Al})$ and $\chi \approx -1.5 \times 10^{-3} \text{\AA}/\text{GPa}$ for $r_b(\text{O2})$
338 (Table 3).

339 The average bonded radius adopted by the Y atom, $\langle r_b(\text{Y}) \rangle = 1.21 \text{\AA}$, at $P = 80.0$ is 0.06 \AA , is
340 smaller than that, 1.27 \AA , adopted at $P = 0.0$. The average bonded radius for the O1 and O2
341 atoms bonded to the Y atoms, $r_b(\text{O1})$ and $r_b(\text{O2})$, is also smaller at $P=80$ GPa, 1.11 \AA than that,
342 1.21 \AA , adopted at $P=0.0$ GPa. Clearly, both atoms are relatively rigid, with the radii decreasing
343 little with increasing pressure with the O atoms being more compressible than the Y atom. The
344 average bonded radius of the Al atoms decreases, on average, from 0.79 \AA to 0.74 \AA while the
345 average radius for the O1 and O2 atoms bonded to the Al decreases from 1.10 \AA to 0.99 \AA as the

346 pressure increases from $P = 0.0$ GPa to 80 GPa. The average bonded radius for the Al atom at
347 $P=0.0$, 0.79 \AA , is slightly smaller than the value, 0.80 \AA , determined by Gibbs et al. (Gibbs et al.,
348 2013), but equal to the radius of the Al atom in the LaAlO_3 perovskite. As evinced by Figure 7,
349 the radius sum of bonded radii $r_b(\text{Al}) + r_b(\text{O})$ and $r_b(\text{Y}) + r_b(\text{O})$ correlate linearly with $R(\text{Al-O})$
350 and $R(\text{Y-O})$, demonstrating that the Al-O and Y-O bond interactions are stable over the range of
351 pressures studied.

352 **Implications**

353 On the basis of bonded radii determined for the silica polymorphs coesite (Gibbs et al., 2003),
354 Prewitt and Downs (1998) reported that the structure of a crystal typically compresses by
355 displaying the largest distortions for the atoms associated with the weakest bonded interactions.
356 They also asserted that the coordination numbers of atoms at high pressure tend to increase with
357 increasing pressure. These rules of thumb are borne out by the observation that the bonded radii
358 of the atoms for stishovite, with the longer Si-O bonded interactions, contract more upon
359 compression, than the bonded radii for the shorter Si-O bonded interactions observed for α - α -
360 quartz. Also the Si atoms are 6-coordinated and the O are 3-coordinated in the high pressure
361 silica polymorph stishovite while the Si and O atoms are 4- and 2-coordinated in α -quartz, well
362 known evidence that high pressure favors the higher coordination numbers for both atoms. It is
363 noteworthy, that an increase in the coordination number of the Y atom of the YAIO_3 perovskite
364 necessarily means that the coordination number of one of the O atoms must necessarily increase
365 as well. It is also clear that that O atoms are more compressible than metal atoms based on the
366 above result that shows the bonded radius of the O atom of stishovite decreases about twice as
367 much, $\sim 0.08 \text{ \AA}$, as the Si atom while the bonded radius of the Si atom only decreases $\sim 0.04 \text{ \AA}$ for
368 an corresponding increase of pressure of 100 GPa. In addition, the bonded radius for the larger,

369 Y atom of $YAlO_3$ perovskite decreases 0.07 \AA , on average, while the O atom bonded to the Y
370 atom decreases slightly more, 0.10 \AA , for a pressure increase of 80.0 GPa. At 20 GPa, the
371 coordination number of Y increases from 8 to 9 while the coordination of O1 increases from 5 to
372 6, as observed above. The bonded radius of the smaller Al atom decreases by 0.05 \AA while the
373 radius of the O atom bonded to the Al decreases 0.10 \AA . In the case of the two remaining
374 $CaSnO_3$ and $LaSnO_3$ perovskites, that were subjected to a much smaller range of pressures
375 between 0 GPa and 15 GPa, the bonded radius of Ca decreases 0.03 \AA and radius of Sn decreases
376 0.02 \AA while the bonded radii of the O atoms bonded to the Ca atoms decrease, 0.04 \AA with the
377 bonded radius of the O atom to Sn decreases 0.02 \AA , on average. For the same pressure range,
378 the bonded radius of the La for $LaAlO_3$, decreases 0.02 \AA while the radius of the O atom bonded
379 to the Y atom decreases 0.05 \AA . In addition, the bonded radius of Al decreases 0.01 \AA while the
380 radius of the O atom bonded to the Al atom decreases 0.02 \AA , on average. On the basis of these
381 results, it is apparent the bonded radii of the atoms for the silica polymorphs and the three
382 perovskites, examined in this study compress a relatively small amount when subjected to
383 pressure, indicating that the metal atoms in these materials are relatively rigid and
384 incompressible compared with the somewhat more compressible O atoms. With the exception of
385 the bonded radius for one of the Y atoms, the compressibilities of Al, Sn, Ca and La atoms in the
386 perovskites and the Si atoms in the silica polymorphs are all less than the O atoms to which they
387 are bonded, again demonstrating that anions are more compressible than metal atoms. The results
388 show that the bonded radii of the atoms for the materials are relatively rigid, with the
389 compressibilities of the smaller atoms, in particular, changing relatively little upon being
390 subjected to pressure, supporting the assertion that pressure has little impact on the sizes of
391 atoms (Grochala et al., 2007). Finally, in the course of undertaking VASP/DFT calculations for a

392 number of molecular, ionic and intrinsically metallic materials, Andreas Hermann and Roald
393 Hoffman (personal communication) have generated a variety of Volume vs. Pressure curves and
394 equations of state, ranging up to pressures of 500 GPa that indicate the atoms like Fe, Au, Ni, W
395 etc. comprising metals and the C atoms in diamond are likewise virtually incompressible and
396 behave as hard sphere atoms at these extremely high pressures. These results and those presented
397 in this report support the argument that high pressure has relatively little impact on the sizes of
398 atoms (Grochala et al., 2007). It is also evident that the small decrease in the bonded radii for
399 atoms at extreme pressures is directly related to changes in the effective interatomic potential
400 with pressure that result in increased repulsion between the nuclei of the bonded atoms as the
401 atoms are squeezed together.

402 **Acknowledgments**

403 NLR acknowledges support from the National Science Foundation (Grant No. EAR-1118691).

404

References

- 405
406
407
408 Angel, R.J., Allan, D.R., Milletich, R., and Finger, L.W. (1997) The use of quartz as an internal
409 pressure standard in high-pressure crystallography. *Journal of Applied Crystallography*,
410 30, 461-466.
- 411 Bader, R.F.W. (1985) Atoms in Molecules. *Accounts of Chemical Research*, 18(1), 9-15.
- 412 Bader, R.F.W. (1990) *Atoms in Molecules: A Quantum Theory*. Oxford University Press, New
413 York, New York.
- 414 Bader, R.F.W. (2009) Bond Paths Are Not Chemical Bonds. *Journal of Physical Chemistry A*,
415 113(38), 10391-10396.
- 416 Bader, R.F.W., and Matta, C.F. (2004) Atomic charges are measurable quantum expectation
417 values: A rebuttal of criticisms of QTAIM charges. *Journal of Physical Chemistry A*,
418 108(40), 8385-8394.
- 419 Gibbs, G.V., Ross, N.L., Cox, D.F., Rosso, K.M., Iversen, B.B., and Spackman, M.A. (2013)
420 Bonded Radii and the Contraction of the Electron Density of the Oxygen Atom by
421 Bonded Interactions. *The Journal of Physical Chemistry A*, 117(7), 1632-1640.
- 422 Gibbs, G.V., Rosso, K.M., Teter, D.M., Boisen Jr, M.B., and Bukowinski, M.S.T. (1999) Model
423 structures and properties of the electron density distribution for low quartz at pressure: a
424 study of the Si O bond. *Journal of Molecular Structure*, 485-486, 13-25.
- 425 Gibbs, G.V., Wang, D., Hin, C., Ross, N.L., Cox, D.F., Crawford, T.D., Spackman, M.A., and
426 Angel, R.J. (2012) Properties of atoms under pressure: Bonded interactions of the atoms
427 in three perovskites. *The Journal of Chemical Physics*, 137(16), 164313.
- 428 Gibbs, G.V., Whitten, A.E., Spackman, M.A., Stimpfl, M., Downs, R.T., and Carducci, M.D.
429 (2003) An exploration of theoretical and experimental electron density distributions and

- 430 Si O bonded interactions for the silica polymorph coesite. *Journal of Physical Chemistry*
431 B, 107(47), 12996-13006.
- 432 Glazer, A. (1972) The classification of tilted octahedra in perovskites. *Acta Crystallographica*
433 Section B, 28(11), 3384-3392.
- 434 Grochala, W., Hoffmann, R., Feng, J., and Ashcroft, N.W. (2007) The chemical imagination at
435 work in very tight places. *Angewandte Chemie-International Edition*, 46(20), 3620-3642.
- 436 Hazen, R.M., Finger, L.W., Hemley, R.J., and Mao, H.K. (1989) High-pressure crystal
437 chemistry and amorphization of alpha-quartz.. *Solid State Communications*, 72(5), 507-
438 511.
- 439 Hill, F.C., Gibbs, G.V., and Boisen, M.B. (1994) Bond Stretching Force-Constants and
440 Compressibilities of Nitride, Oxide, and Sulfide Coordination Polyhedra in Molecules
441 and Crystals. *Structural Chemistry*, 5(6), 349-355.
- 442 Nicoll, J.S., Gibbs, G.V., Boisen, M.B., Downs, R.T., and Bartelmehs, K.L. (1994) Bond length
443 and radii variations in fluoride and oxide molecules and crystals. *Physics and Chemistry*
444 *of Minerals*, 20(8), 617-624.
- 445 Prencipe M., Nestola F. (2006). Minerals at high pressure. Mechanics of compression from
446 quantum mechanical calculations in a case study: the beryl ($\text{Al}_4\text{Be}_6\text{Si}_{12}\text{O}_{36}$). *Physics and*
447 *Chemistry of Minerals*, 34, 37–52.
- 448 Prewitt, C.T., and Downs, R.T. (1998) High-pressure crystal chemistry. In R.J. Hemley, Ed.
449 *Ultra-high-Pressure Mineralogy: Physics and Chemistry of the Earth's Deep Interior*, 37,
450 p. 283-317. Mineralogical Soc America, Washington.
- 451 Ross, N.L., Shu, J.F., Hazen, R.M., and Gasparik, T. (1990) High-Pressure Crystal-Chemistry of
452 Stishovite. *American Mineralogist*, 75(7-8), 739-747.

- 453 Ross, N.L., Zhao, J., and Angel, R.J. (2004) High-pressure single-crystal X-ray diffraction study
454 of YAlO_3 perovskite. *Journal of Solid State Chemistry*, 177(4-5), 1276-1284.
- 455 Runtz, G.R., Bader, R.F.W., and Messer, R.R. (1977) Definition of Bond Paths and Bond
456 Directions in Terms of Molecular Charge-Distribution. *Canadian Journal of Chemistry-*
457 *Revue Canadienne De Chimie*, 55(16), 3040-3045.
- 458 Sasaki, S., Fujino, K., Takeuchi, Y., and Sadanaga, R. (1980) On the estimation of atomic
459 charges by the X-ray method for some oxides and silicates. *Acta Crystallographica*
460 Section A, 36(6), 904-915.
- 461 Shannon, R.D., and Prewitt, C.T. (1969) Effective Ionic Radii in Oxides and Fluorides. *Acta*
462 *Cryst.*, B25, 925-946.
- 463 Wang, D. (2012) Some aspects of the crystal chemistry of perovskites under high pressures.
464 Geosciences, PhD. Virginia Polytechnic Institute and State University, Blacksburg, VA.
- 465 Woodward, P. (1997) Octahedral Tilting in Perovskites. I. Geometrical Considerations. *Acta*
466 *Crystallographica Section B*, 53(1), 32-43.
- 467 Zhao, J., Ross, N.L., and Angel, R.J. (2004) Tilting and distortion of CaSnO_3 perovskite to 7
468 GPa determined from single-crystal X-ray diffraction. *Physics and Chemistry of*
469 *Minerals*, 31(5), 299-305.

470

471

472

Figure Captions

473

474 Figure 1. Plot of the bonded radii, r_b (Å) of the Si (blue and red circles) and O (blue and red
475 diamonds) atoms in α -quartz between 1 bar and 30 GPa and the Si (red and black solid circles)
476 and O (blue and red squares) atoms in stishovite between 0 and 100 GPa.

477 Figure 2. Plot of the bonded radii, r_b (Å), of the La and O atoms in LaAlO_3 between 0 and 15
478 GPa.

479 Figure 3. Plot of the La-O and Al-O distances, $R(\text{M-O})$ (Å), in LaAlO_3 as a function of the sum
480 of the bonded radii of the metal atoms (La and Al) and oxygen atom, $r_b(\text{M})+r_b(\text{O})$ (Å).

481 Figure 4. Plot of the bonded radii, r_b (Å), of the Ca and O atoms in CaSnO_3 between 0 and 15
482 GPa.

483 Figure 5. Plot of the Ca-O and Sn-O distances, $R(\text{M-O})$ (Å), in CaSnO_3 as a function of the sum
484 of the bonded radii of the metal atoms (Ca and Sn) and oxygen atom, $r_b(\text{M})+r_b(\text{O})$ (Å).

485 Figure 6. Plot of the bonded radii, r_b (Å), of the Y and O atoms in YAlO_3 between 0 and 80 GPa.

486 Figure 7. Plot of the Y-O and Al-O distances, $R(\text{M-O})$ (Å), in YAlO_3 as a function of the sum of
487 the bonded radii of the metal atoms (Y and Al) and oxygen atom, $r_b(\text{M})+r_b(\text{O})$ (Å).

488

489

Table 1. Calculated bond lengths (Å), critical bond radii for the La atom, $rb(M)$ (Å), and O atom, $rb(O)$ (Å), and electron density at bond critical points, $\rho(Rc)$ ($e/\text{Å}^3$) for LaAlO_3 perovskite between 0 and 15 GPa.

M-O	P (GPa):	0	1.18	2.78	4.63	6.81	8.62	10	12	15
La-Oi	R(M-O)	2.4756	2.4750	2.4752	2.4758	2.4761	2.4769	2.4776	2.4785	2.4807
	$rb(M)$	1.350	1.350	1.350	1.351	1.351	1.351	1.352	1.352	1.353
	$rb(O)$	1.125	1.125	1.125	1.125	1.125	1.126	1.126	1.126	1.128
	$\rho(Rc)$	0.3432	0.3438	0.3441	0.3441	0.3444	0.3442	0.3441	0.3440	0.3430
La-Oii	R(M-O)	2.6560	2.6509	2.6443	2.6369	2.6285	2.6219	2.6169	2.6101	2.6001
	$rb(M)$	1.431	1.429	1.426	1.423	1.419	1.416	1.414	1.411	1.407
	$rb(O)$	1.225	1.222	1.219	1.214	1.209	1.206	1.203	1.199	1.193
	$\rho(Rc)$	0.2417	0.2443	0.2484	0.2523	0.2569	0.2605	0.2632	0.2668	0.2725
La-Oiii	R(M-O)	2.8419	2.8324	2.8189	2.8035	2.7863	2.7721	2.7613	2.7465	2.7238
	$rb(M)$	1.509	1.505	1.499	1.493	1.486	1.480	1.476	1.470	1.460
	$rb(O)$	1.333	1.328	1.320	1.310	1.300	1.292	1.285	1.277	1.263
	$\rho(Rc)$	0.1683	0.1716	0.1764	0.1820	0.1887	0.1942	0.1985	0.2044	0.2136
Al-O	R(M-O)	1.8857	1.8818	1.8767	1.8709	1.8644	1.8593	1.8554	1.8501	1.8423
	$rb(M)$	0.791	0.789	0.788	0.786	0.784	0.782	0.781	0.779	0.777
	$rb(O)$	1.095	1.092	1.089	1.085	1.081	1.077	1.074	1.071	1.066
	$\rho(Rc)$	0.4559	0.4598	0.4650	0.4710	0.4780	0.4836	0.4879	0.4938	0.5027

Table 2. Calculated bond lengths (Å), critical bond radii for the Ca atom, rb(M) (Å), and O atom, rb(O) (Å), and electron density at bond critical points, $\rho(Rc)$ ($e/\text{Å}^3$) for CaSnO_3 perovskite between 0 and 15 GPa.

M-O (Å)	P (GPa):	0	0.738	1.5	2.61	3.94	5.18	5.98	6.73	10	12	15
Ca-O1i	R(M-O)	2.2786	2.2742	2.2697	2.2635	2.2563	2.2497	2.2456	2.2419	2.2263	2.2172	2.2045
	rb(M)	1.147	1.146	1.144	1.141	1.138	1.135	1.134	1.132	1.125	1.121	1.116
	rb(O)	1.131	1.129	1.126	1.122	1.118	1.114	1.112	1.110	1.101	1.096	1.088
	$\rho(Rc)$	0.3209	0.3239	0.3271	0.3315	0.3368	0.3417	0.3448	0.3476	0.3597	0.3670	0.3774
Ca-O1ii	R(M-O)	2.3548	2.3510	2.3467	2.3414	2.3347	2.3286	2.3249	2.3215	2.3067	2.2981	2.2857
	rb(M)	1.180	1.178	1.176	1.174	1.172	1.169	1.168	1.166	1.160	1.156	1.151
	rb(O)	1.175	1.173	1.170	1.167	1.163	1.160	1.157	1.155	1.147	1.142	1.134
	$\rho(Rc)$	0.2794	0.2817	0.2843	0.2877	0.2919	0.2959	0.2983	0.3006	0.3107	0.3166	0.3255
Ca-O2i	R(M-O)	2.2994	2.2952	2.2908	2.2852	2.2783	2.2719	2.2682	2.2647	2.2499	2.2414	2.2294
	rb(M)	1.157	1.155	1.153	1.151	1.148	1.145	1.144	1.142	1.136	1.132	1.127
	rb(O)	1.143	1.140	1.138	1.134	1.130	1.127	1.125	1.123	1.114	1.109	1.102
	$\rho(Rc)$	0.3081	0.3110	0.3140	0.3179	0.3228	0.3273	0.3300	0.3326	0.3436	0.3502	0.3597
Ca-O2ii	R(M-O)	2.5746	2.5702	2.5685	2.5611	2.5557	2.5499	2.5458	2.5424	2.5282	2.5194	2.5073
	rb(M)	1.270	1.268	1.267	1.264	1.262	1.260	1.258	1.257	1.252	1.248	1.244
	rb(O)	1.305	1.302	1.301	1.297	1.293	1.290	1.287	1.285	1.277	1.271	1.264
	$\rho(Rc)$	0.1728	0.1745	0.1752	0.1780	0.1802	0.1825	0.1841	0.1855	0.1913	0.1951	0.2005
Ca-O2iii	R(M-O)	2.7950	2.7903	2.7834	2.7776	2.7682	2.7601	2.7555	2.7511	2.7315	2.7205	2.7040
	rb(M)	1.360	1.358	1.356	1.353	1.350	1.347	1.345	1.343	1.336	1.332	1.326
	rb(O)	1.436	1.433	1.428	1.425	1.419	1.414	1.411	1.408	1.396	1.389	1.379
	$\rho(Rc)$	0.1090	0.1101	0.1117	0.1132	0.1154	0.1175	0.1187	0.1198	0.1249	0.1279	0.1325
Sn-O1	R(M-O)	2.0679	2.0651	2.0621	2.0584	2.0538	2.0496	2.0472	2.0448	2.0350	2.0294	2.0214
	rb(M)	1.062	1.061	1.059	1.058	1.055	1.054	1.052	1.051	1.047	1.044	1.041
	rb(O)	1.006	1.004	1.003	1.001	0.998	0.996	0.995	0.994	0.988	0.985	0.981
	$\rho(Rc)$	0.6087	0.6122	0.6160	0.6209	0.6270	0.6325	0.6359	0.6390	0.6524	0.6603	0.6716
Sn-O2i	R(M-O)	2.0608	2.0583	2.0559	2.0525	2.0486	2.0450	2.0427	2.0407	2.0322	2.0272	2.0204

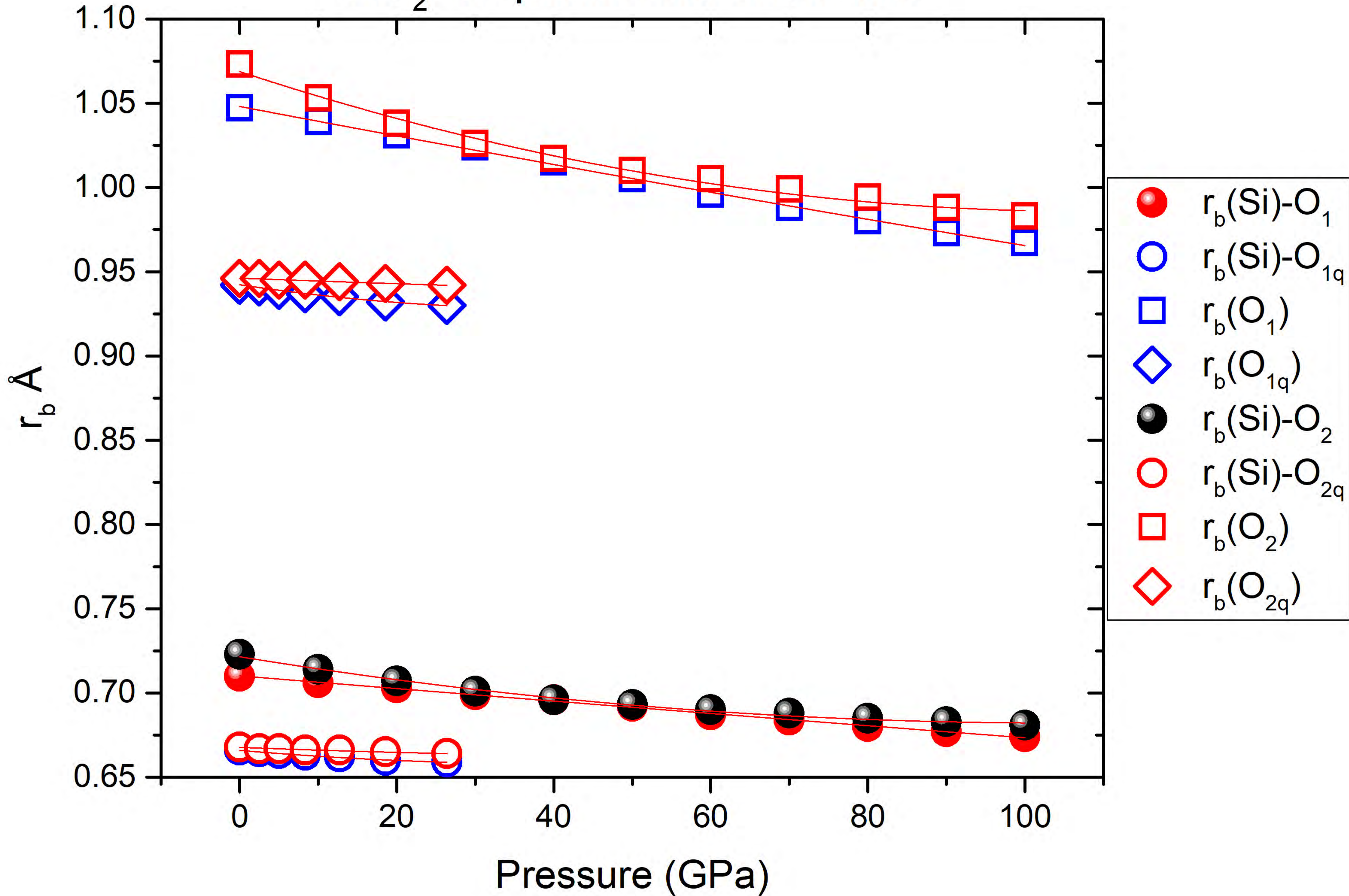
	rb(M)	1.059	1.058	1.057	1.055	1.053	1.052	1.051	1.050	1.046	1.043	1.040
	rb(O)	1.002	1.001	0.999	0.998	0.995	0.993	0.992	0.991	0.987	0.984	0.980
	ρ (Rc)	0.6166	0.6199	0.6230	0.6275	0.6326	0.6374	0.6404	0.6431	0.6547	0.6616	0.6713
Sn-O2ii	R(M-O)	2.0642	2.0619	2.0595	2.0565	2.0527	2.0493	2.0472	2.0453	2.0372	2.0326	2.0261
	rb(M)	1.061	1.060	1.058	1.057	1.055	1.054	1.053	1.052	1.048	1.046	1.043
	rb(O)	1.004	1.002	1.001	1.000	0.997	0.996	0.995	0.994	0.989	0.987	0.983
	ρ (Rc)	0.6127	0.6157	0.6188	0.6228	0.6278	0.6324	0.6352	0.6378	0.6489	0.6553	0.6646

Table 3. Calculated bond lengths (Å), critical bond radii for the Y atom, rb(M) (Å), and O atom, rb(O) (Å), and electron density at bond critical points, $\rho(Rc)$ ($e/\text{Å}^3$) for YAlO_3 perovskite between 0 and 80 GPa.

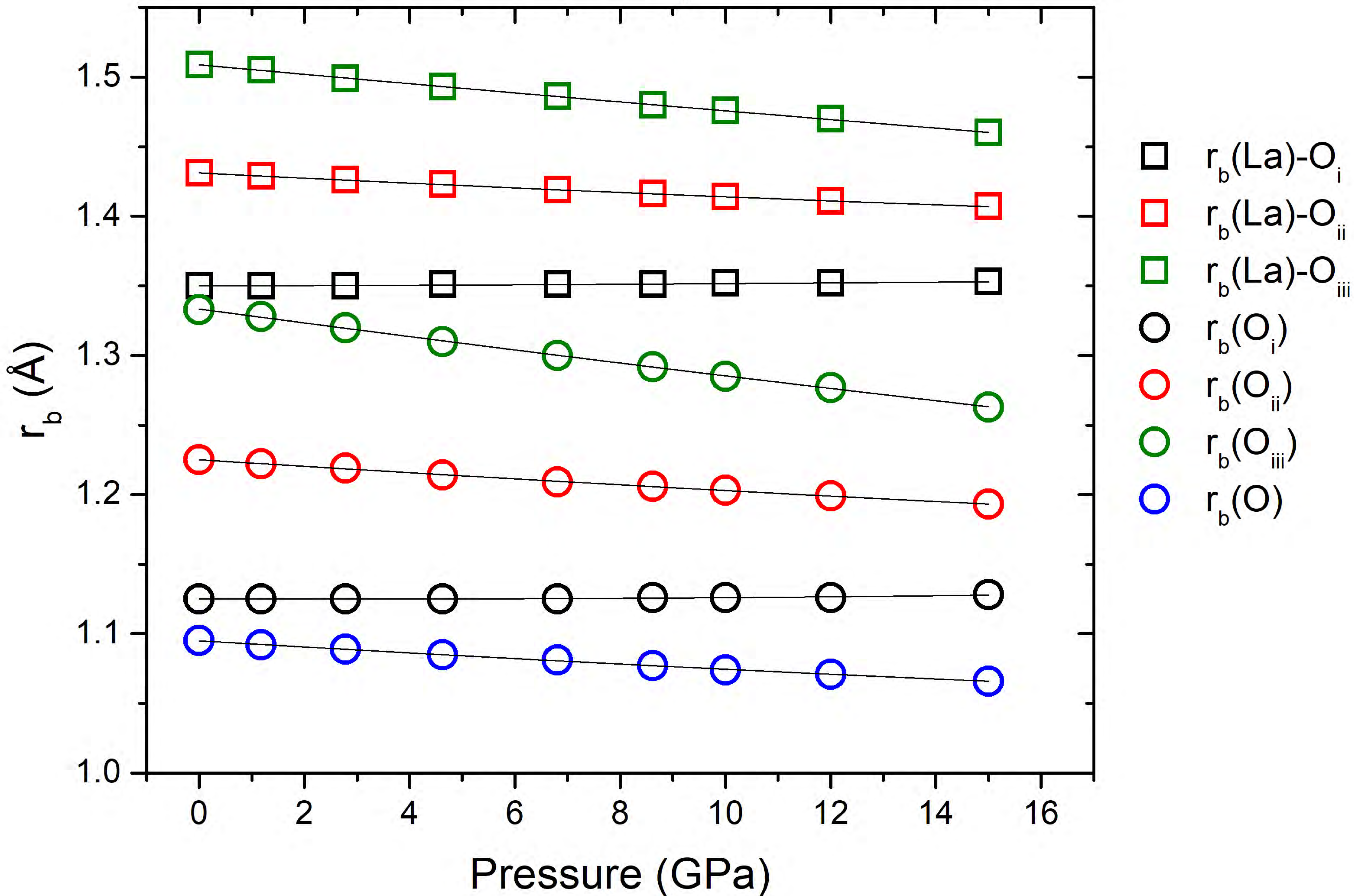
M-O	P (GPa):	0	1.05	2.59	3.791	5.09	6.31	7.11	7.94	10	12	15	20	40	60	80
Y-O1i	R(M-O)	2.2213	2.2187	2.2147	2.2118	2.2088	2.2059	2.2042	2.2023	2.1977	2.1935	2.1874	2.1782	2.1462	2.1204	2.0975
	rb(M)	1.165	1.164	1.162	1.161	1.159	1.158	1.157	1.156	1.154	1.152	1.149	1.145	1.130	1.118	1.107
	rb(O)	1.056	1.055	1.053	1.051	1.049	1.048	1.047	1.046	1.044	1.041	1.038	1.033	1.016	1.003	0.991
	$\rho(Rc)$	0.4652	0.4679	0.4721	0.4751	0.4782	0.4813	0.4832	0.4851	0.4901	0.4947	0.5015	0.5120	0.5505	0.5842	0.6163
Y-O1ii	R(M-O)	2.2839	2.2827	2.2808	2.2793	2.2779	2.2768	2.2758	2.2749	2.2732	2.2712	2.2689	2.2653	2.2565	2.2518	2.2489
	rb(M)	1.195	1.195	1.194	1.193	1.193	1.192	1.192	1.191	1.191	1.190	1.189	1.187	1.183	1.181	1.180
	rb(O)	1.088	1.088	1.087	1.086	1.085	1.085	1.084	1.083	1.083	1.081	1.080	1.078	1.073	1.071	1.069
	$\rho(Rc)$	0.4110	0.4121	0.4137	0.4150	0.4162	0.4172	0.4181	0.4189	0.4204	0.4220	0.4240	0.4272	0.4353	0.4397	0.4427
Y-O1iii	R(M-O)	2.9720	2.9663	2.9583	2.9522	2.9457	2.9399	2.9361	2.9322	2.9230	2.9143	2.9019	2.8830	2.8232	2.7818	2.7530
	rb(M)	1.487	1.485	1.481	1.479	1.476	1.474	1.472	1.470	1.467	1.463	1.459	1.451	1.428	1.413	1.402
	rb(O)	1.491	1.488	1.482	1.478	1.474	1.470	1.468	1.465	1.459	1.454	1.446	1.434	1.396	1.370	1.352
	$\rho(Rc)$	0.0990	0.1000	0.1016	0.1028	0.1041	0.1053	0.1061	0.1069	0.1089	0.1108	0.1136	0.1180	0.1337	0.1459	0.1557
Y-O1iv	R(M-O)	Null	Null	Null	Null	Null	Null	Null	Null	Null	Null	Null	2.9466	2.8077	2.6948	2.6038
	rb(M)	Null	Null	Null	Null	Null	Null	Null	Null	Null	Null	Null	1.485	1.418	1.371	1.334
	rb(O)	Null	Null	Null	Null	Null	Null	Null	Null	Null	Null	Null	1.478	1.391	1.324	1.270
	$\rho(Rc)$	Null	Null	Null	Null	Null	Null	Null	Null	Null	Null	Null	0.1003	0.1314	0.1660	0.2017
Y-O2i	R(M-O)	2.2551	2.2520	2.2477	2.2444	2.2410	2.2379	2.2359	2.2338	2.2287	2.2240	2.2172	2.2068	2.1718	2.1455	2.1256
	rb(M)	1.181	1.180	1.178	1.176	1.175	1.173	1.172	1.171	1.169	1.167	1.164	1.159	1.143	1.131	1.121
	rb(O)	1.074	1.072	1.070	1.068	1.066	1.065	1.064	1.062	1.060	1.057	1.053	1.048	1.029	1.015	1.004
	$\rho(Rc)$	0.4380	0.4408	0.4449	0.4481	0.4514	0.4545	0.4565	0.4585	0.4636	0.4684	0.4754	0.4863	0.5252	0.5566	0.5820
Y-O2ii	R(M-O)	2.4310	2.4287	2.4253	2.4228	2.4201	2.4176	2.4160	2.4144	2.4106	2.4067	2.4015	2.3931	2.3633	2.3357	2.3067
	rb(M)	1.258	1.257	1.255	1.254	1.253	1.252	1.251	1.251	1.249	1.247	1.245	1.242	1.228	1.216	1.204
	rb(O)	1.173	1.172	1.170	1.169	1.167	1.166	1.165	1.164	1.162	1.159	1.156	1.152	1.135	1.119	1.103
	$\rho(Rc)$	0.2954	0.2971	0.2992	0.3009	0.3026	0.3043	0.3053	0.3064	0.3087	0.3112	0.3148	0.3205	0.3426	0.3640	0.3881
Y-O2iii	R(M-O)	2.5574	2.5530	2.5469	2.5422	2.5372	2.5329	2.5300	2.5270	2.5202	2.5136	2.5045	2.4907	2.4474	2.4174	2.3977
	rb(M)	1.316	1.314	1.311	1.310	1.308	1.306	1.305	1.303	1.301	1.298	1.295	1.289	1.271	1.259	1.251
	rb(O)	1.241	1.239	1.235	1.233	1.230	1.227	1.225	1.224	1.219	1.215	1.210	1.202	1.176	1.158	1.147
	$\rho(Rc)$	0.2245	0.2271	0.2301	0.2325	0.2350	0.2372	0.2388	0.2403	0.2437	0.2472	0.2522	0.2600	0.2864	0.3062	0.3205
Al-O1	R(M-O)	1.8855	1.8822	1.8775	1.8739	1.8702	1.8668	1.8646	1.8623	1.8569	1.8518	1.8445	1.8333	1.7948	1.7635	1.7364
	rb(M)	0.790	0.789	0.787	0.786	0.785	0.784	0.783	0.783	0.781	0.779	0.777	0.773	0.761	0.751	0.742

	rb(O)	1.096	1.093	1.090	1.088	1.085	1.083	1.081	1.080	1.076	1.073	1.068	1.060	1.034	1.012	0.994
	ρ (Rc)	0.4591	0.4624	0.4672	0.4708	0.4747	0.4783	0.4806	0.4830	0.4889	0.4945	0.5027	0.5156	0.5635	0.6073	0.6492
Al-O2i	R(M-O)	1.8949	1.8918	1.8872	1.8838	1.8803	1.8769	1.8747	1.8725	1.8669	1.8617	1.8541	1.8422	1.7999	1.7657	1.7377
	rb(M)	0.793	0.792	0.790	0.789	0.788	0.787	0.786	0.786	0.784	0.782	0.780	0.776	0.763	0.752	0.743
	rb(O)	1.102	1.100	1.097	1.095	1.092	1.090	1.089	1.087	1.083	1.080	1.074	1.066	1.037	1.014	0.995
	ρ (Rc)	0.4522	0.4551	0.4596	0.4630	0.4666	0.4700	0.4723	0.4746	0.4804	0.4860	0.4942	0.5076	0.5591	0.6061	0.6487
Al-O2ii	R(M-O)	1.9095	1.9057	1.9003	1.8962	1.8918	1.8879	1.8853	1.8827	1.8763	1.8704	1.8617	1.8485	1.8029	1.7673	1.7385
	rb(M)	0.798	0.796	0.795	0.793	0.792	0.791	0.790	0.789	0.787	0.785	0.783	0.778	0.764	0.752	0.743
	rb(O)	1.112	1.109	1.106	1.103	1.100	1.097	1.095	1.094	1.089	1.085	1.079	1.070	1.039	1.015	0.995
	ρ (Rc)	0.4339	0.4374	0.4427	0.4467	0.4510	0.4550	0.4576	0.4602	0.4669	0.4732	0.4824	0.4972	0.5528	0.6021	0.6463

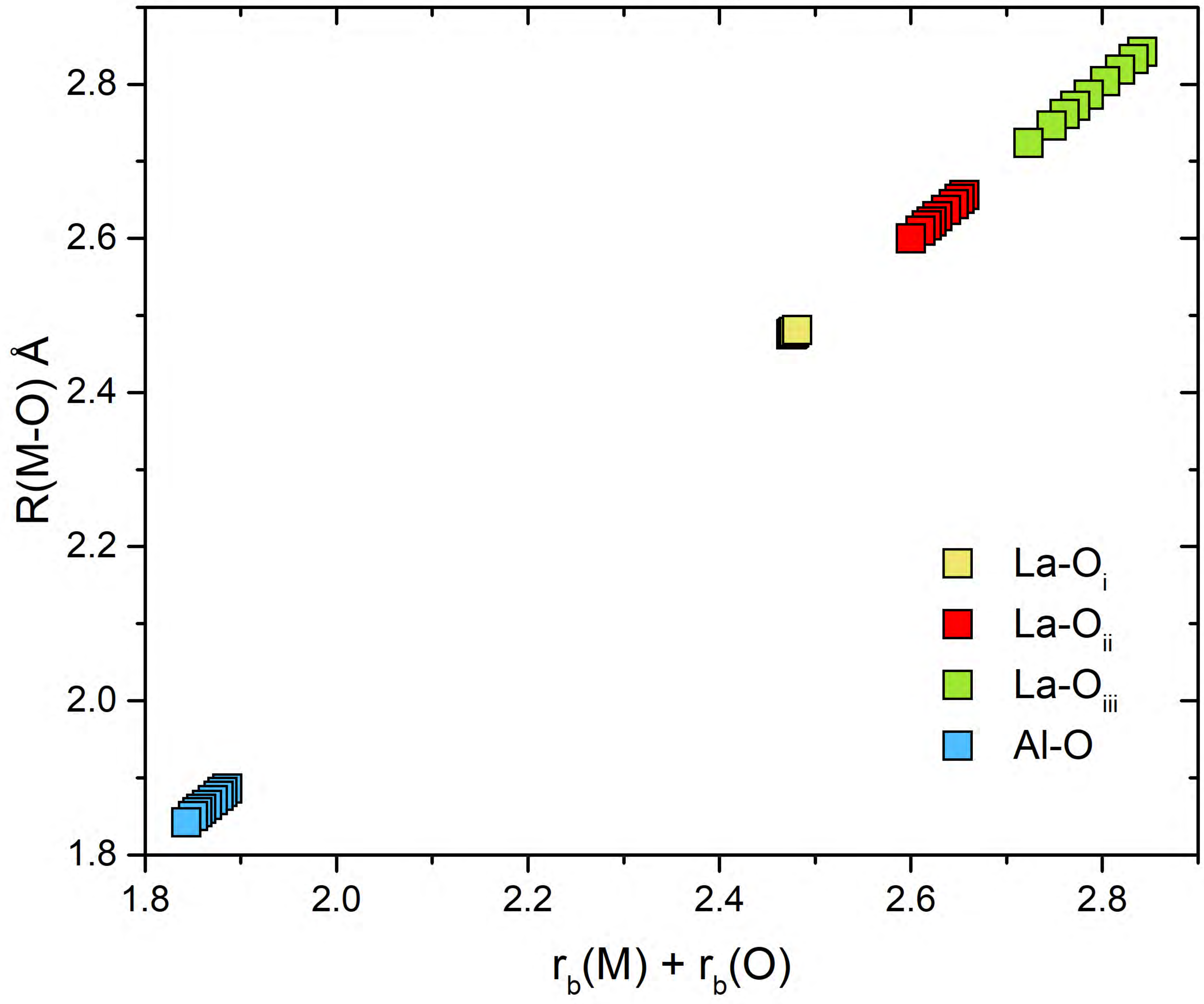
SiO₂: α -quartz and stishovite



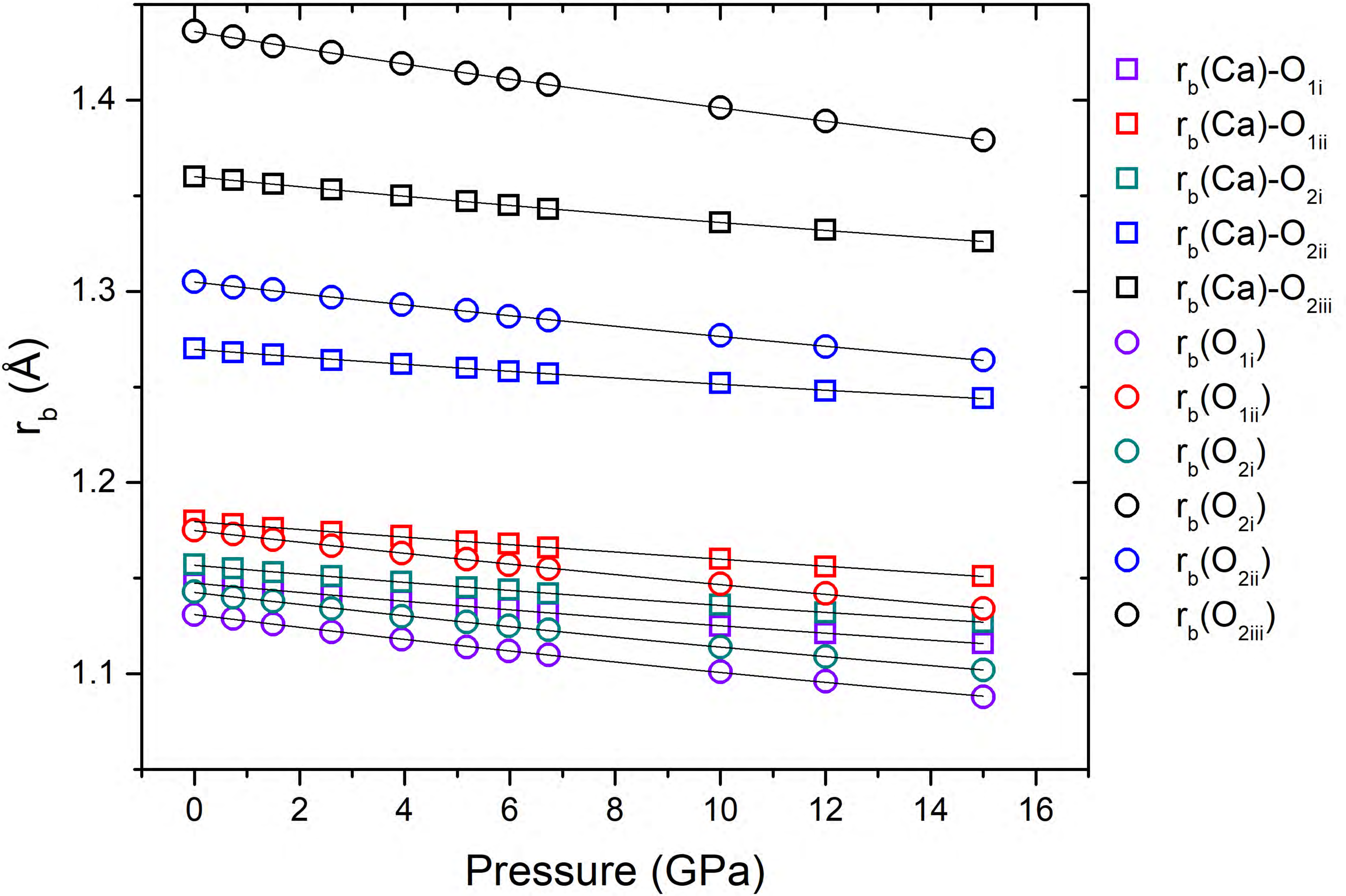
LaAlO₃



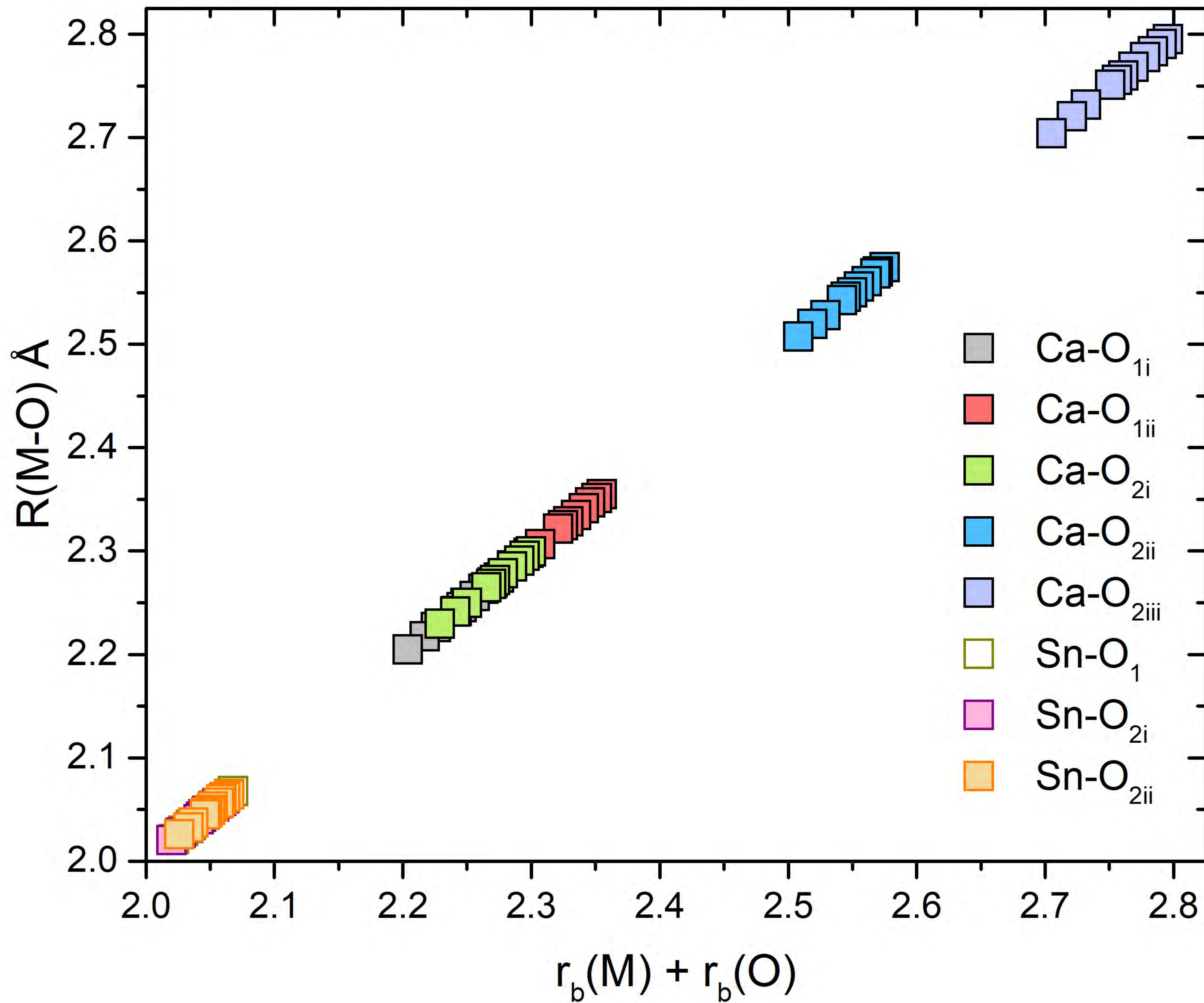
LaAlO₃



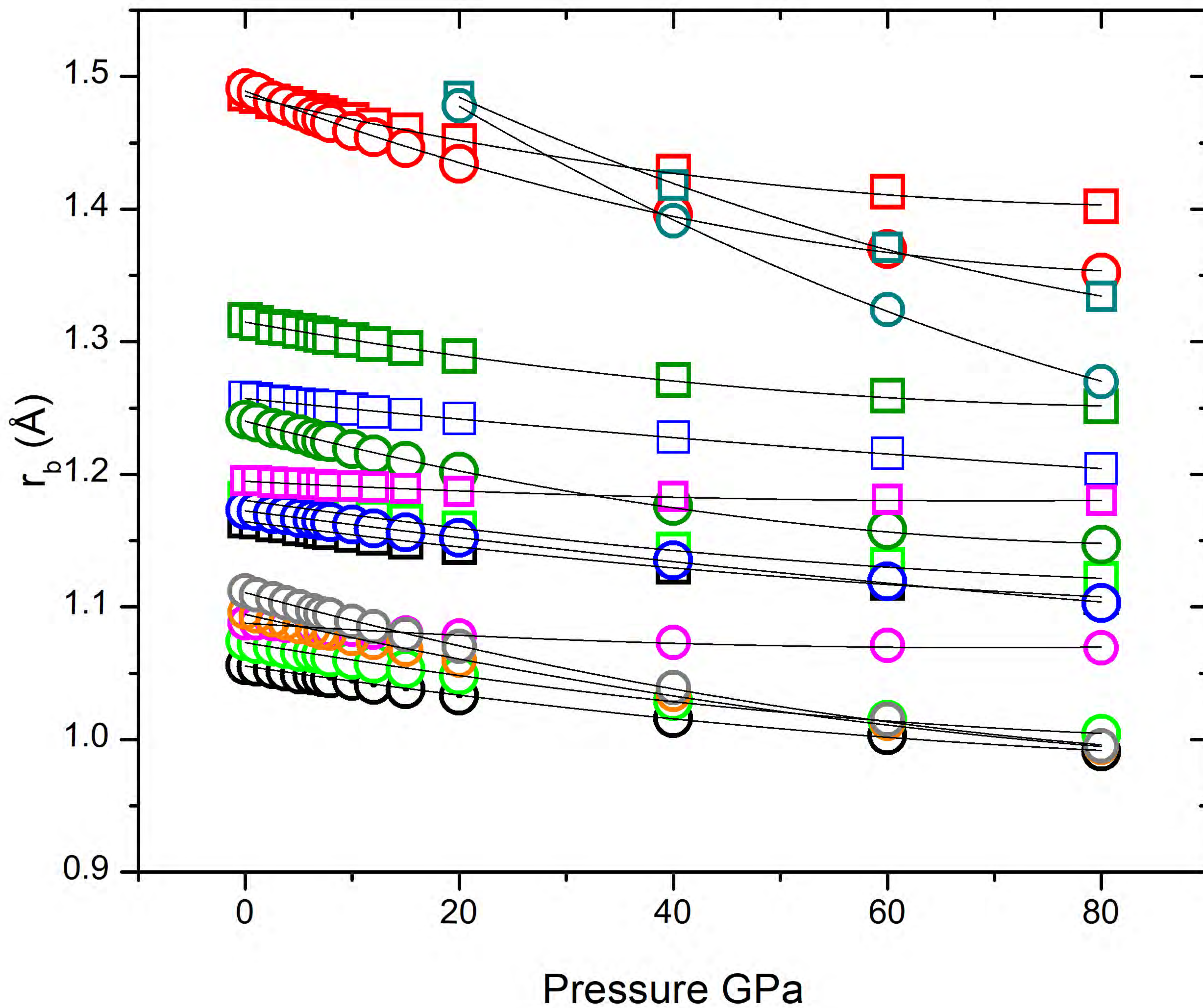
CaSnO₃



CaSnO₃



YAIO₃



YAIO₃

